

### **PAPER • OPEN ACCESS**

# Demonstrating tungsten fiber-reinforced porousmatrix tungsten composites for future fusion application

To cite this article: Yiran Mao et al 2022 Nucl. Fusion 62 106029

View the article online for updates and enhancements.

# You may also like

- Towards plasma cleaning of ITER first mirrors
- L. Moser, L. Marot, B. Eren et al.
- Development of advanced high heat flux and plasma-facing materials
   Ch. Linsmeier, M. Rieth, J. Aktaa et al.
- Fracture behavior of random distributed short tungsten fiber-reinforced tungsten
- composites
  Y. Mao, J.W. Coenen, J. Riesch et al.

Nucl. Fusion 62 (2022) 106029 (10pp)

# Demonstrating tungsten fiber-reinforced porous-matrix tungsten composites for future fusion application

Yiran Mao<sup>1,2</sup>, Jan W. Coenen<sup>2,3</sup>, Alexis Terra<sup>2</sup>, Liang Gao<sup>2,\*</sup>, Arkadi Kreter<sup>2</sup>, Marius Wirtz<sup>2</sup>, Chao Liu<sup>4</sup>, Chang Chen<sup>5</sup>, Johann Riesch<sup>6</sup>, Yucheng Wu<sup>1,5</sup>, Christoph Broeckmann<sup>4</sup> and Christian Linsmeier<sup>2</sup>

- School of Mechanical Engineering, Hefei University of Technology, Hefei 230009, People's Republic of China
- <sup>2</sup> Forschungszentrum Jülich GmbH, Institut für Energie- und Klimaforschung Plasmaphysik, Partner in the Trilateral Euregio Cluster, 52425 Jülich, Germany
- <sup>3</sup> Department of Engineering Physics, University of Wisconsin Madison, WI 53706, Madison, United States of America
- <sup>4</sup> Institut für Werkstoffanwendungen im Maschinenbau (IWM), RWTH Aachen University, 52062 Aachen, Germany
- <sup>5</sup> Intelligent Manufacturing of HFUT, Hefei University of Technology, Hefei 230009, People's Republic of China
- <sup>6</sup> Max-Planck-Institut für Plasmaphysik, 85748 Garching b. München, Germany

E-mail: li.gao@fz-juelich.de

Received 3 May 2022, revised 28 July 2022 Accepted for publication 24 August 2022 Published 16 September 2022



### **Abstract**

Tungsten fiber-reinforced tungsten (W<sub>f</sub>/W) has been developed to improve the fracture toughness of W materials, as demonstrated in previous studies (2019 Nucl. Fusion 59 086034; 2021 Mater. Sci. Eng. A 817 141361). In the present study, we focus on the performance of the developed W<sub>f</sub>/W materials under fusion-relevant test conditions and further demonstrate their use as plasma facing materials in future fusion reactors. Specifically, one set of W<sub>f</sub>/W samples was exposed to Ne plasma to investigate the erosion resistance against plasma sputtering, in comparison to the reference ITER-grade W sample. In addition, deuterium (D) retention in the plasma-exposed W<sub>f</sub>/W samples was studied via thermal desorption spectroscopy. Furthermore, laser thermal shock tests were performed on W<sub>f</sub>/W to simulate the transient heat load condition and to investigate the material performance under extreme heat flux. With increasing porosity, W<sub>f</sub>/W exhibits lower mass loss (net erosion) after Ne plasma exposure. Though porous, W<sub>f</sub>/W composites unexpectedly show a comparable D retention to the reference bulk W, which is attributed to the openness of the pores in the matrix. Thermal shock testing results indicate a similar cracking threshold (0.38 GW m<sup>-2</sup>, 1 ms) as compared with that of ITER-grade W materials. However, due to the lower thermal conductivity of porous matrix W<sub>f</sub>/W, under extremely high loading conditions (1.6 GW m<sup>-2</sup>, 2 ms) surface melting was observed. The present work demonstrates the great potential of the porous matrix  $W_f/W$  for future fusion application.

Original content from this work may be used under the terms of the Creative Commons Attribution 4.0 licence. Any further distribution of this work must maintain attribution to the author(s) and the title

distribution of this work must maintain attribution to the author(s) and the title of the work, journal citation and DOI.

<sup>\*</sup>Author to whom any correspondence should be addressed.

Keywords: tungsten fiber-reinforced tungsten, short fibers, porous matrix, plasma erosion, deuterium retention, laser thermal shock

(Some figures may appear in colour only in the online journal)

### 1. Introduction

For use as plasma-facing materials (PFM) in future fusion reactors, candidates require advanced mechanical and thermal properties [3] to meet significant challenges in harsh environments. This is the case particularly in the divertor region, where surfaces are subjected to extensive particle and heat fluxes. Tungsten is one of the most suitable materials for use as PFM in the divertor region due to its favorable physical properties, such as low sputtering yield, high sputtering threshold, high thermal conductivity and high melting point. However, the intrinsic brittleness of W materials has strongly limited their applications in fusion reactors. This brittleness issue is foreseen to be further worsened when exposed to fusion plasma with neutron irradiation [4-7]. Intensive efforts have been devoted to overcoming the brittleness of tungsten or enhancing the fracture toughness. Toughening techniques can be divided into two groups, i.e., intrinsic and extrinsic toughening. The former principle includes adding nanoparticles [8, 9], grain refinement [10], and alloying [11]; while techniques applying composites, e.g., multilayer composites [12, 13] and tungsten fiber-reinforced composites [14–16], belong to extrinsic toughening mechanisms. Given the fact that cracking is almost inevitable in the harsh fusion environments with neutron embrittlement, the extrinsic toughening strategy seems to be more applicable for W materials. Relying on the extrinsic toughening mechanism [17], various types of tungsten fiber-reinforced tungsten composites (W<sub>f</sub>/W) have been developed in the past few years [2, 16, 18–22], e.g., W<sub>f</sub>/W contents 30% fiber mass fraction and an yttrium oxide interface between fibers and dense matrix to realize the toughening effect [16]. The improved fracture toughness relies on the extra energy consumption mechanisms (e.g., crack deflection, interface debonding, fiber ductile deformation, etc) enabled by the weak bonding between the fibers and matrix. In previous studies [16, 20, 23] on W<sub>f</sub>/W, the weak bonding was mainly realized by a dedicated oxide interface. However, the introduction of the oxide interfaces turned out to be costly and technically challenging, and has therefore strongly limited the large-scale production of W<sub>f</sub>/W. Recently, a new concept of porous matrix W<sub>f</sub>/W (PoMa-W<sub>f</sub>/W), with typically 80%–88% relative density tungsten matrix, has been proposed and fabricated [2, 22] applying a controlled matrix porosity instead of introducing oxide interface to realize the weak connection between fibers and the matrix [24]. It has been demonstrated [2] that such novel PoMa-W<sub>f</sub>/W materials exhibit significantly improved fracture toughness and crack resistance compared with pure W. More importantly, it does not require the dedicated yttrium oxide coating to realize the weak bonding between fiber and

matrix, and thereby promising great potential in large-scale production for future application in fusion reactors.

In our previous work [2], it has been reported that PoMa-W<sub>f</sub>/W exhibits an increased fracture toughness compared to pure W relying on the extrinsic toughening mechanism. In the present study, to further demonstrate the suitability of applying PoMa-W<sub>f</sub>/W as PFMs in future fusion reactor, we investigate the materials performance under plasma exposure with focus on hydrogen isotopes retention and erosion [3, 25–27]. Specifically, PoMa-W<sub>f</sub>/W with different relative density have been produced and exposed to deuterium (D) plasma at the linear plasma device PSI-2 in Forschungszentrum Juelich [28]. The D retention after plasma exposure was probed using thermal desorption spectroscopy (TDS). Neon (Ne) plasma was applied to study the erosion behavior of W<sub>f</sub>/W under plasma exposure. In addition, the cracking behavior of the PoMa-W<sub>f</sub>/W under transient heat load is studied. Pulsed laser was shot to sample surfaces to simulate the transient heat load during fusion operations.

### 2. Experimental

### 2.1. Sample preparation

Pure tungsten powders (OSRAM GmbH) with 5  $\mu$ m average particle size and potassium doped short tungsten fibers (OSRAM GmbH) with 2.4 mm length and 0.15 mm diameter were employed as the raw materials to manufacture PoMa-W<sub>f</sub>/W via field assisted sintering technology [22]. Fibers with a very fine and elongated grain structure, due to the drawing process upon production, show good elongation (up to  $\sim 3\%$ ) and extremely high tensile strength (up to 3000 MPa) [29]. In addition, during the production, potassium ( $\sim$ 75 ppm) doping is used to strengthen the microstructural stability. Potassium is insoluble in tungsten, forming dispersed nanobubble rows along the grain boundaries of the elongated grains, which can resist the growth of grains during recrystallization [30]. It has been reported that even after annealing at  $\sim$ 2170 K for 30 min, the potassium-doped W fibers can still show ductile behavior during tensile testing at room temperature [30].

For the consolidation process, short tungsten fibers and powders were mixed by manual shaking in a vessel. The mixture was then spread into a columnar graphite mold with 20 mm in diameter. Tungsten foils with a thickness of 0.025 mm were used between the to be sintered sample and the graphite mold to mitigate possible carbon contamination during sintering process [31]. To acquire W<sub>f</sub>/W samples with different matrix porosity, various sintering temperatures were used, as listed in table 1. The sintering was performed in vacuum with a base pressure below 0.1 mbar. As a result,

Table 1.	Sample	production	parameters.

	$W_f/W_{\#1}$	$W_f/W_{\#2}$	$W_f/W_{\#3}$	Reference W
Sintering temperature	∼1820 K	∼1670 K	~2170 K	_
Pressure	60 MPa	60 MPa	60 MPa	_
Fiber mass fraction	40%	40%	30%	_
Density	$\sim$ 85%	$\sim 78\%$	$\sim$ 93%	$\sim$ 99%

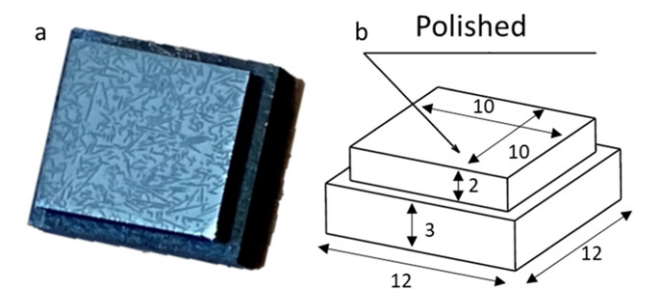


**Figure 1.** (a) Typical  $W_f/W$  irradiation sample, the dark particles are the short fibers; (b) sample geometry of plasma exposure and laser shock in PSI-2.

coin-shape samples (20 mm in diameter and  $\sim$ 6 mm in height) were produced. Here, the reference W in this work was made from sintering followed by a forging process manufactured by Plansee, according to ITER specifications with average (SEM measured) grain size between 1 and 10  $\mu$ m, slightly elongated perpendicularly to the exposed surface. A more detailed characterization can be found in [32]. This reference W here has been a widely investigated as the candidate for plasma facing material. The reason of choosing this material as the reference W is due to the fact that we would like to demonstrate the potential of using  $W_f/W$  as plasma facing material and compare the correlating behavior with other 'standard' candidates.

Afterwards, the samples were cut into standardized shaped samples for testing in PSI-2 device with a dimension shown in figure 1, using electrical discharge machining. The sample surfaces were afterwards mechanically ground and polished until 0.25  $\mu m$  (polishing particle size) for a mirror finish. After polishing, the Ra of the reference W and W<sub>f</sub>/W<sub>#1</sub>, W<sub>f</sub>/W<sub>#2</sub> and W<sub>f</sub>/W<sub>#3</sub> are 19 nm, 1355 nm, 393 nm and 239 nm, respectively; the Rz are 134 nm, 22 406 nm, 11 542 nm and 19 550 nm respectively. The reason for the high surface roughness of the PoMa-W<sub>f</sub>/W is due to the relatively large height difference between the fiber and matrix after polishing and nature of high roughness of the porous surface.

The typical microstructure of the prepared  $W_f/W$  samples is shown in figure 2. Randomly oriented and distributed fibers can be seen in the tungsten matrix, which is in a porous state and shown in figure 2(b). For more details on the microstructure of the PoMa- $W_f/W$ , the reader is referred to our previous study [2].

### 2.2. Plasma erosion

To investigate the plasma erosion resistance, PoMa-W<sub>f</sub>/W and reference pure W were exposed to Ne plasma in PSI-2 device with active water cooling in the backside of the sample. The

sample temperature during Ne plasma exposure was monitored by a thermal couple attached to the backside of the sample. The average bias voltage between the neon plasma and the samples was 108 eV; the total exposure fluence was  $3.65 \times 10^{24}~\text{Ne}^+~\text{m}^{-2}$ . During the exposure, the sample temperature was  $\sim\!320~\text{K}$ .

The sample masses before and after Ne plasma exposure were measured by micro-balance to access the mass loss caused by the plasma erosion. The evolution of sample surface morphology due to erosion experiments was characterized using scanning electron microscope (SEM, Zeiss DSM 982).

### 2.3. Deuterium retention

An independent set of samples (including PoMa-W<sub>f</sub>/W and reference W) were exposed to deuterium (D) plasma at PSI-2 devices to study the retention behavior of hydrogen isotopes in PoMa-W<sub>f</sub>/W. Before the D plasma exposure, all the samples were annealed at 1270 K for 100 min in order to degas and release the residual stress. Experimental conditions were set similarly to the above-mentioned Ne plasma exposure, except for the incident ion species. The average bias voltage between the D plasma and the samples was 78 eV; the total fluence was  $4.99 \times 10^{25} \, \mathrm{D^+ m^{-2}}$ . During the exposure, sample temperature was stabilized at around 470 K, which was monitored using a thermal couple attached to the back side of the sample.

After D plasma exposure, the samples were stored in a vacuum chamber  $(10^{-2} \text{ mbar})$  for 6 months. Afterwards, the total deuterium retention was measured by TDS up to 1000 K in 'TESS' [33] at IPP Garching Germany, where the sample was heated with a linear temperature ramp of 3 K min<sup>-1</sup> and the released D-containing molecules are measured by quadrupole mass spectroscopy, including HD (mass 3),  $D_2$  (mass 4), HDO (mass 19),  $D_2$ O (mass 20), and other mass channels, but only HD and  $D_2$  were later taken into account for the quantification of D amount due to the difficulty in calibrations HDO and  $D_2$ O signal. The QMS signal for  $D_2$  was calibrated to absolute desorption fluxes by an independent measurement using a calibrated leak (Laco Technologies). The calibration factor for HD is taken as a factor of 0.6 as that for  $D_2$  signal.

### 2.4. Laser thermal shock

To investigate the materials behavior under transient heat load condition, laser beam exposure was applied in PSI-2 device. A Nd:YAG laser (LASAG FLS 352 N) was used ( $\lambda = 1064$  nm), with absorbed power densities between 0.19 GW m<sup>-2</sup> and 1.6 GW m<sup>-2</sup> [34]. The power profile of the laser beam is identical with the profile in [34]. A circular area with a diameter of 3.6 mm was exposed to 1–1000 pulses, with a pulse duration

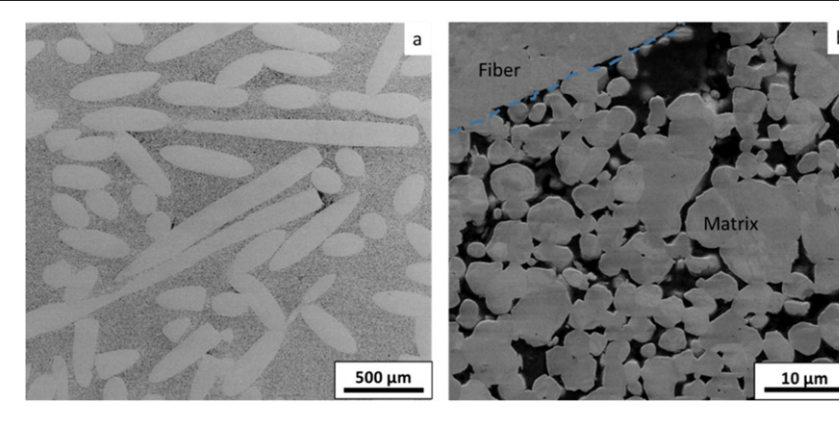


Figure 2. Typical microstructure of PoMa-W<sub>f</sub>/W (85% relative density).

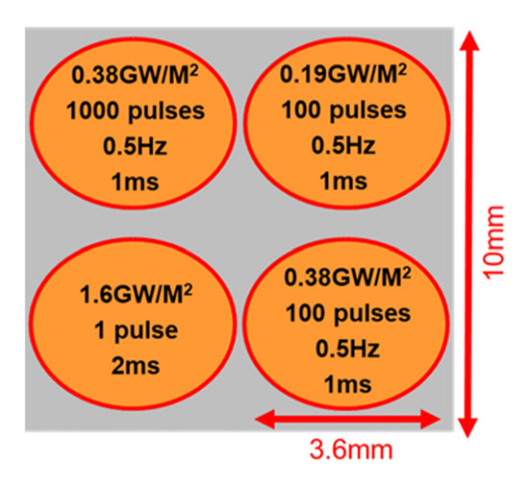


Figure 3. Schematic diagram of thermal shock spot on W and  $W_f/W$  samples.

of 1–2 ms. The pulse frequencies were 0.5 Hz in order to allow sample cooling down to room temperature after each pulse. For each sample, four spots were tested with different power densities, pulse numbers or durations. The laser shots parameters on each spot are shown in figure 3. The surface morphology after the laser beam shock was analyzed by SEM (Zeiss, Crossbeam 540) equipped with focus ion beam (FIB) for cross-sectioning.

### 3. Results and discussion

## 3.1. Plasma erosion

One major concern upon applying porous matrix for PFM is the possible particle flaking under bombardments of energetic ions. On the one hand, particle flaking leads to additional weight loss beyond that induced by plasma erosion. The exfoliated particles or pieces will impose a lot of impurities into the core plasma and may lead to plasma disruption. High net erosion and particle shedding will both limit the life time of plasma facing component and therefore should be avoided.

Assuming a normal incidence for all the impacting particles, the theoretical mass loss from a flat surface due to plasma

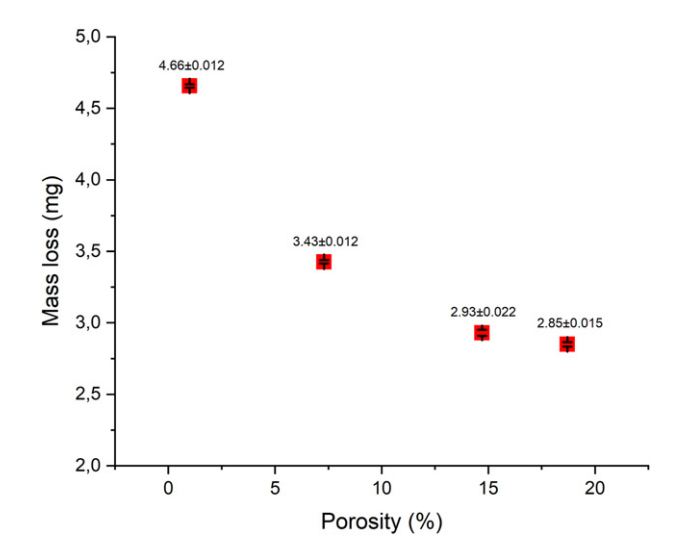


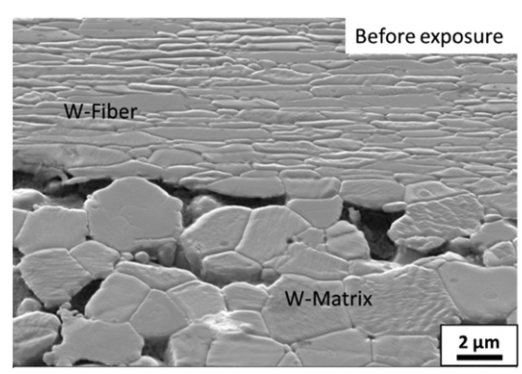
Figure 4. Weight loss vs porosity after Ne plasma (108 eV) irradiation for pure W and  $W_f/W$  with different matrix density.

sputtering can be calculated by [35]:

$$\Delta m_{\text{weight}} = \Phi \cdot Y \cdot S \cdot m_{\text{W}}. \tag{1}$$

Where  $\Delta m_{\text{weight}}$  is the theoretical mass loss,  $\Phi$  the incident particle fluence, Y the sputtering yield at given ion energy, S the surface area,  $m_{\text{W}}$  the mass of the tungsten atom.

Applying the sputtering yield of W by 100 eV Ne ions in [35], the theoretical mass loss of pure W during the Ne plasma exposure is calculated as 4.0 mg. It should be pointed out that in equation (1) redeposition of sputtered particles is not considered. In other words, the experimentally measured weight loss after plasma erosion should be typically lower than that calculated by equation (1) due to redeposition of sputtered particles. In our experiments, the mass losses caused by plasma erosion for both the reference W sample and several PoMa-W<sub>f</sub>/W samples with different porosity are measured, as plotted in figure 4. The reference W sample is plotted just assuming a 1% porosity, which shows slightly higher mass loss compared to the theoretical value (4 mg). This is attributed to the sputter erosion induced by other impurity ion species contained in the PSI-2 plasma beam during neon plasma operation [36], which is not considered in equation (1). However,



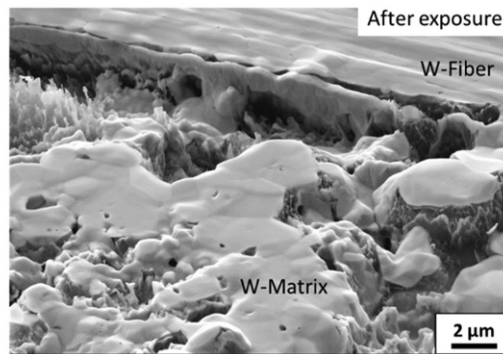
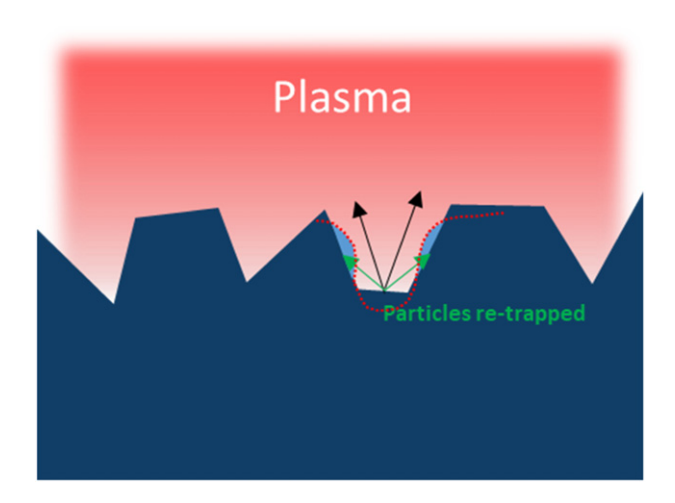


Figure 5. Surface morphology of  $W_f/W$  (85% relative density) before and after Ne plasma irradiation. In order to manifest the surface roughness more clearly, the samples are tilted for 54° here.



**Figure 6.** Illustration of surface roughness influence on the plasma erosion effect, dashed line marked the possible surface after erosion.

for the  $W_f/W$  with different porosities (figure 4), the mass losses are less than the theoretical value, despite the influence of the impurities. This indicates a relatively strong redeposition occurring on PoMa- $W_f/W$  surfaces. Another interesting aspect in figure 4 is the decreasing trend of the mass loss as a function of the sample porosity, which will be discussed in next paragraph.

To understand the lower net erosion of PoMa-W<sub>f</sub>/W, surface morphologies of samples with different porosity were characterized using SEM. Figure 5 represents the typical surface morphology of W<sub>f</sub>/W sample (85% relative density) before and after Ne plasma exposure. Due to the high porosity, the surface before exposure looks already quite rough; pores/gaps between the tungsten grains are visible. Fine grain structures of tungsten fibers can also be seen on the surface as the smooth part. After Ne plasma exposure, great changes have taken place for the porous W matrix in terms of surface morphology. Grassy features have formed in the gaps and edges of single particle become roundish, similar to the results in [37]. These grassy features are typical morphology after redeposition. For tungsten fibers with flat surface areas present in the exposed surface, no significant change can be distinguished before and after Ne plasma exposure, demonstrating a less effective redeposition.

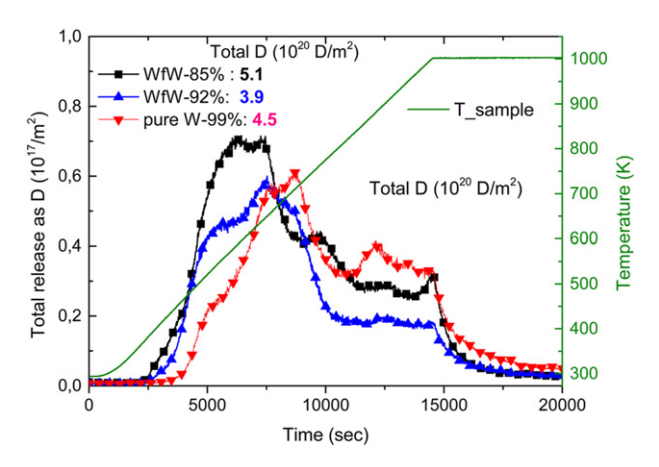


Figure 7. D retention measured by TDS test up to 1000 K (3 K s $^{-1}$ , green) for the sample  $W_f/W$  with 85% density (black), 92% density (blue) and reference W (red).

Based on the above results, the lower mass loss of PoMa- $W_f/W$  samples compared with the theoretical value can be referred to the re-deposition effect due to high surface roughness of the matrix. As sketched in figure 6, when the surface roughness is high, the particles being sputtered away can be re-trapped by the surface bumps with much higher probability, as it has been reported in [38, 39]. Additionally, according to the less mass loss of PoMa- $W_f/W$ , together with the SEM observation, the loose matrix structure does not cause the shedding of W particles under plasma erosion.

### 3.2. Deuterium retention

Besides the concern on possible higher erosion upon applying porous materials as plasma facing components, another major worry is the fuel retention in the porous structure [40, 41]. To measure the D retention in the PoMa-W $_f$ /W materials, samples were exposed to D plasma together with a reference W, followed by a TDS measurement up to 1000 K.

The D-release spectra measured by TDS for PoMa- $W_f/W$  and reference W are shown in figure 7. All three spectra exhibit multi-peak structure and span over a large temperature range. D desorption spectrum of the PoMa- $W_f/W$  samples start at temperature of  $\sim 400 \, \text{K}$  while the reference W starts at  $\sim 450 \, \text{K}$ . Typically, the release-starting temperature in TDS signal can

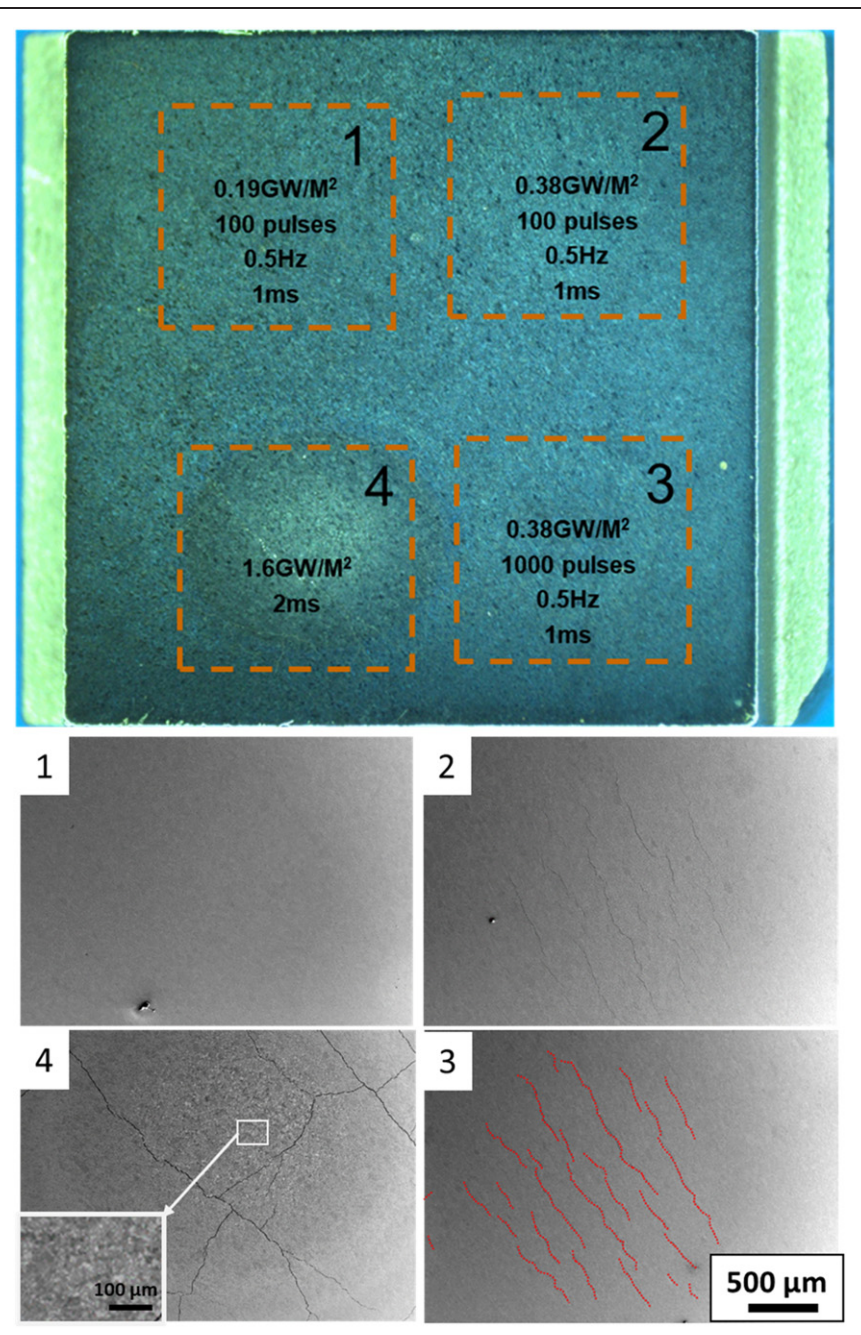


Figure 8. Surface morphology of reference W after laser thermal shock testing.

be corresponded to the sample temperature at the end of exposure to hydrogen. In our case, once the plasma beam is switched off, the sample starts cooling. But  $D_2$  gas injection has not been ceased immediately. It is highly probable that samples can absorb some  $D_2$  gas at the surfaces and the pores for the cases of PoMa-W<sub>f</sub>/W. We attributed the D release at temperature slightly below the exposure temperature ( $\sim$ 470 K) to the absorbed part during the cooling process. Our focus via the TDS measurements are on comparing the total amount of retained D in the samples. As labelled in the legend of figure 7, the total amount of retained D in W<sub>f</sub>/W with 85% (5.1  $\times$  10<sup>20</sup> D m<sup>-2</sup>) and 92% (3.9  $\times$  10<sup>20</sup> D m<sup>-2</sup>) density are comparable to that in reference W (4.5  $\times$  10<sup>20</sup> D m<sup>-2</sup>). Given the fact that there are many pores in both W<sub>f</sub>/W samples, the

comparable D retention can only be attributed to the openness of these pores (i.e., pore networks) in the matrix [31]. With open pore networks, the implanted D particles will easily be reemitted or they can penetrate throughout the sample [42]. Therefore, the high porosity will not cause higher D retention compared to the dense bulk W. This is stressed as the most important finding in the present work.

### 3.3. Laser thermal shock

Apart from erosion and fuel retention, another worry when using PoMa-W<sub>f</sub>/W as plasma facing materials is its relatively lower thermal conductivity due to high porosity. As reported in [2], the thermal conductivity of PoMa-W<sub>f</sub>/W is considerably

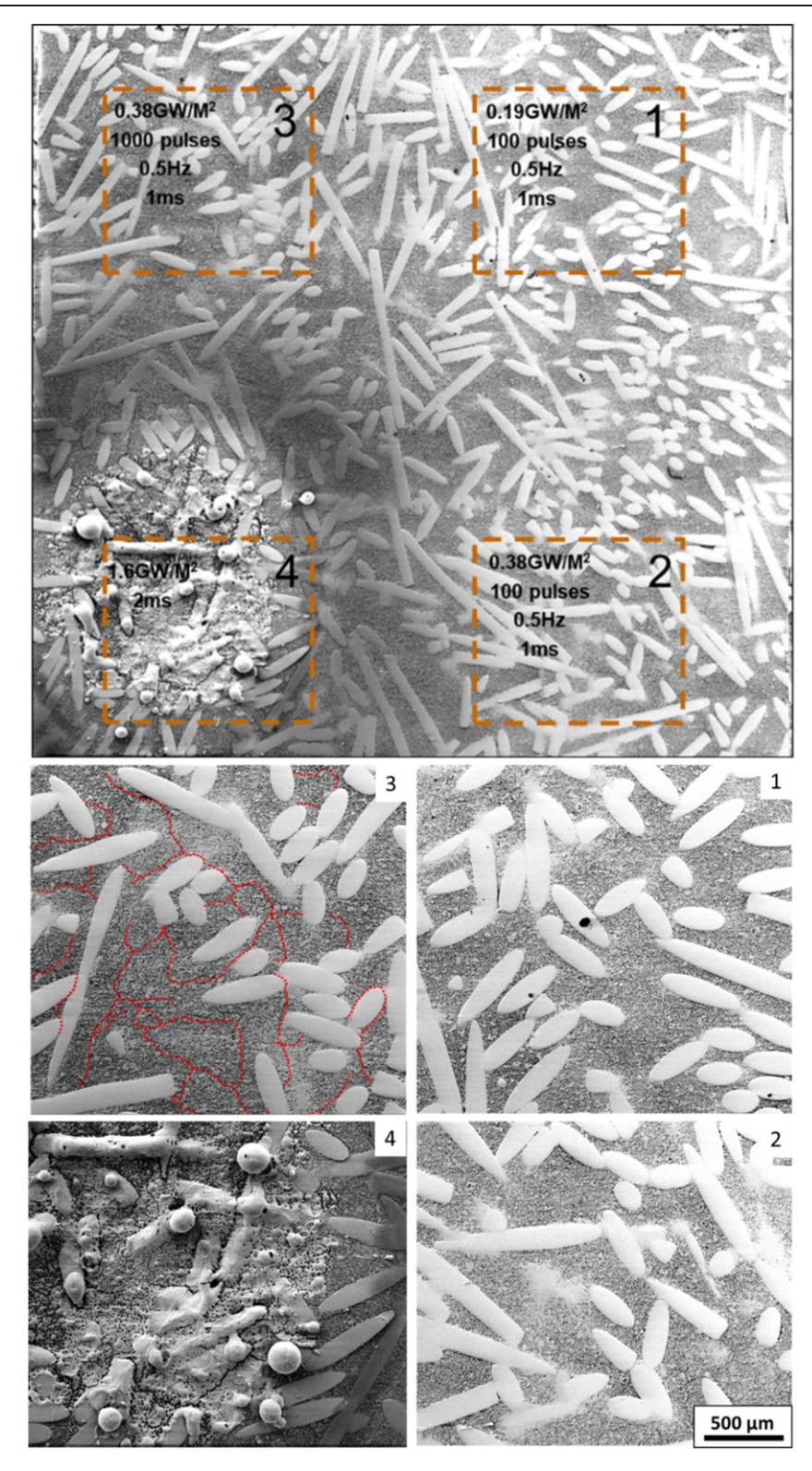


Figure 9. Surface morphology of PoMa-W<sub>f</sub>/W (80% relative density) after laser thermal shock testing.

lower than the bulk W. This lower thermal conductivity could lead to higher thermal stress [43] and, in very high loading condition, surface melting, especially for the case of transient heat load condition in future fusion operation.

To study the performance of PoMa-W<sub>f</sub>/W materials under high thermal loads/stresses, pulsed laser beam shock was

applied. During each laser pulse, the locally heated spot tends to expand due to thermal expansion and shrink during cooling. On the other hand, the unheated adjacent area around shocked spot restricts the expansion and shrinkage, which leads to high stress and fatigue for cycled loading [44]. This could cause crack initiation in tungsten as reported in [45]. The test aims

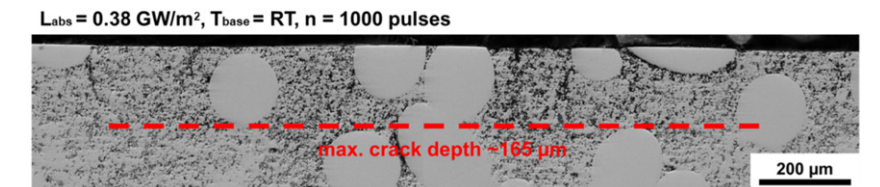


Figure 10. Cross section of  $W_f/W$  (85% relative density) after laser beam shock with a loading condition of 0.38 GW m<sup>-2</sup> for 1 ms with a pulse number of 1000 (spot 3).

to simulate the material behavior under high thermal stress and fatigue under cycled exposures in future fusion operation. After pulsed laser shock, the surface morphologies of reference W and typical PoMa- $W_f$ /W are shown in figures 8 and 9. In both figures, the four shock spots are magnified to display the crack formation. To emphasize the typical crack profile, the cracks are marked by red dash lines for spots 3.

For reference W, for spot 1 (figure 8(1), 0.19 GW m<sup>-2</sup>, 100 pulse), no cracks or any surface morphology changing are observed. With a power density of 0.38 GW m<sup>-2</sup> for 100 cycles (spot 2, figure 8(2)), cracks appear in a straight parallel pattern. After 1000 cycles with the same power density (spot 3, figure 8(3)), no significant change can be observed in terms of cracking morphology in comparison with that after 100 cycles (spot 2, figure 8(2)). When the sample is loaded with an extremely high power of 1.6 GW m<sup>-2</sup> for a long duration of 2 ms (figure 8(4)), large cracking networks were built-up instead of the parallel pattern. A careful comparison with that in spot 2 & 3 (figures 8(2) and (3)) gives rise to an enhanced surface roughness and also lager grain size, indicating the occurrence of recrystallization. According to previous thermal fatigue study on W [46], the damage threshold for ITER-grade W under heat load is between 0.19 GW m<sup>-2</sup> and 0.38 GW m<sup>-2</sup>. The observed results in terms of crack formation and surface morphology evolution after laser thermal shock testing are consistent with the previous study.

For PoMa-W<sub>f</sub>/W (figure 9), the damaging behavior of PoMa-W<sub>f</sub>/W under laser thermal shock is in general very similar to reference W. Similar damage threshold (between 0.19 to 0.38 GW m<sup>-2</sup>) in terms of crack appearance is found (see figures 9(2) and (3)). The number of cracks is also comparable for PoMa-W<sub>f</sub>/W and reference W. However, the cracking pattern at the exposed surface is rather a network in PoMa-W<sub>f</sub>/W than straight lines in reference W sample. This is a clear sign of crack deflection that can be attributed to tungsten fibers. Namely, cracks appear only within the matrix, no crack can pass through any W-fiber by a careful search. These aspects demonstrate our proposal on extrinsic strengthening, when applying short W fibers in porous matrix. Further testing on PoMa-W<sub>f</sub>/W materials with much higher power density and pulse duration (1.6 GW m<sup>-2</sup>, 2 ms) gives rise to surface melting (see spot 4, figure 9(4)). This phenomenon is not observed for the reference W sample with the same loading condition (figure 8(4)). It is attributed to the lower thermal conductivity of PoMa-W<sub>f</sub>/W.

In order to further demonstrate the cracking behavior of PoMa- $W_f/W$ , cross section of the laser shock spot (0.38 GW m<sup>-2</sup> for 1 ms with a pulse number of 1000) was

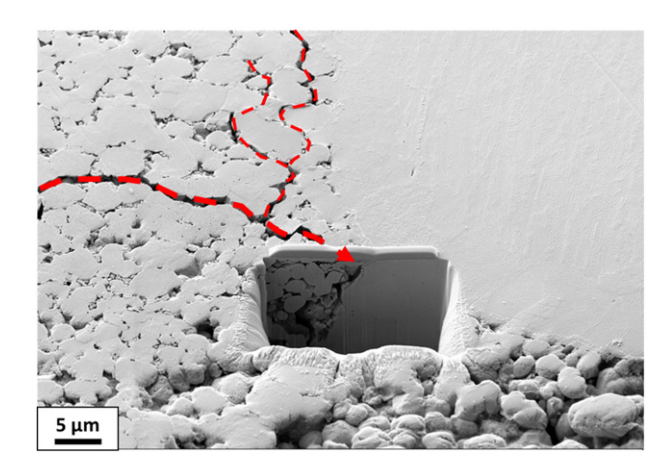


Figure 11. SEM image showing crack stopped by the fibers for  $W_f/W$  (92% relative density), sample preparation prepared by FIB cut.

observed, as shown in figure 10. Additionally, the cracking path is traced in figure 11. Here a small crack cross section is prepared by focused ion beam (FIB).

From figure 10, the maximum crack depth is measured as  $\sim 165 \, \mu \mathrm{m}$  for this sample, which is in the same range compared to pure W in previous studies [46, 47]. Additionally, it can be seen that the cracks are not in a sharp manner. They are passivated due to the porous matrix. Compared to a sharp crack in a normal tungsten, the stress concentration at the passivated crack tip is much lower [48], hindering the further crack propagation. From figure 11, one can see that the cracks are deflected by a fiber. This mechanism is often reported in the fiber-reinforced composites. The deflected cracks lead to larger cracking surface, consuming higher fracture energy.

To sum up, although PoMa-W<sub>f</sub>/W has to suffer a higher thermal stress due to lower thermal conductivity, apart from under the extremely high loading condition, the cracking behavior is still comparable to ITER-grade W, as both cases give a similar cracking threshold with similar numbers of cracks. This can be attributed to two effects: (a) the crack tip passivation due to the porous matrix and (b) the crack deflection by the tungsten fibers. Considering the much higher high fracture toughness of PoMa-W<sub>f</sub>/W, the initiated surface cracks cannot easily propagate through the material causing unexpected failure, which gives a promising advantage when using PoMa-Wf/W as the plasma facing materials.

### 4. Conclusion

Our previous work demonstrated the much higher fracture toughness of W<sub>f</sub>/W compared to pure W [1], especially after

neutron irradiation [49]. The present work further studies the performance of the developed PoMa-W<sub>f</sub>/W materials under fusion-relevant exposure conditions. Our testing experiments of PoMa-W<sub>f</sub>/W materials on erosion resistance during Ne irradiation, D retention after D plasma exposure and cracking threshold by laser thermal shock show better or at least similar results in comparison with those from reference bulk W samples. The generally positive results have largely eliminated the worries possibly induced by the applied porous matrix, such as particle flaking, rather high hydrogen fuel retention, etc. The severe melting of PoMa-W<sub>f</sub>/W materials under extreme loading condition (1.6 GW m<sup>-2</sup> for 2 ms), being the solely observable drawback under the applied testing conditions, is attributed to the lower thermal conductivity due to the porous matrix. However, since such extreme heat load is also rare and should be avoided during the operation of future fusion reactors, we deem that the observed melting is less relevant to future fusion application compared with other tested properties. Therefore, the developed PoMa-W<sub>f</sub>/W, allowing for largescale production, is a promising candidate for application in a future fusion reactor.

### **Acknowledgments**

This work has been carried out within the framework of the EUROfusion Consortium, funded by the European Union via the Euratom Research and Training Programme (Grant Agreement No. 101052200—EUROfusion). Views and opinions expressed are however those of the author(s) only and do not necessarily reflect those of the European Union or the European Commission. Neither the European Union nor the European Commission can be held responsible for them. This work is supported by 'the Fundamental Research Funds for the Central Universities', project (Grant No. JZ2020HGQB0230), the International Cooperation Fund of Anhui Province (202104b11020023), the International Postdoctoral Exchange Fellowship Program of Helmholtz-OCPC (No. 20191010).

### **ORCID iDs**

Yiran Mao https://orcid.org/0000-0002-5518-2791

Jan W. Coenen https://orcid.org/0000-0002-8579-908X

Alexis Terra https://orcid.org/0000-0003-0638-6103

Liang Gao https://orcid.org/0000-0003-2514-8514

Arkadi Kreter https://orcid.org/0000-0003-3886-1415

Marius Wirtz https://orcid.org/0000-0002-1857-688X

Johann Riesch https://orcid.org/0000-0001-6896-6352

Christian Linsmeier https://orcid.org/0000-0003-0404-7191

### References

 [1] Mao Y. et al 2019 Fracture behavior of random distributed short tungsten fiber-reinforced tungsten composites Nucl. Fusion 59 086034

- [2] Mao Y. et al 2021 Design of tungsten fiber-reinforced tungsten composites with porous matrix Mater. Sci. Eng. A 817 141361
- [3] Philipps V. 2011 Tungsten as material for plasma-facing components in fusion devices J. Nucl. Mater. 415 S2–9
- [4] Pintsuk G., Bobin-Vastra I., Constans S., Gavila P., Rödig M. and Riccardi B. 2013 Qualification and post-mortem characterization of tungsten mock-ups exposed to cyclic high heat flux loading *Fusion Eng. Des.* 88 1858–61
- [5] Coenen J.W. et al 2017 Advanced materials for a damage resilient divertor concept for DEMO: powder-metallurgical tungsten-fibre reinforced tungsten Fusion Eng. Des. 124 964–8
- [6] Li M. and You J.-H. 2015 Interpretation of the deep cracking phenomenon of tungsten monoblock targets observed in high-heat-flux fatigue tests at 20 MW m<sup>-2</sup> Fusion Eng. Des. 101 1–8
- [7] Bolt H., Barabash V., Federici G., Linke J., Loarte A., Roth J. and Sato K. 2002 Plasma facing and high heat flux materials—needs for ITER and beyond J. Nucl. Mater. 307–311 43–52
- [8] Xie Z.M. et al 2015 Extraordinary high ductility/strength of the interface designed bulk W–ZrC alloy plate at relatively low temperature Sci. Rep. 5 16014
- [9] Luo L., Shi J., Lin J., Zan X., Zhu X., Xu Q. and Wu Y. 2016 Microstructure and performance of rare earth elementstrengthened plasma-facing tungsten material *Sci. Rep.* 6 32701
- [10] Zhang Y., Ganeev A.V., Wang J.T., Liu J.Q. and Alexandrov I.V. 2009 Observations on the ductile-to-brittle transition in ultrafine-grained tungsten of commercial purity *Mater. Sci. Eng.* A 503 37–40
- [11] Ren C., Fang Z.Z., Koopman M., Butler B., Paramore J. and Middlemas S. 2018 Methods for improving ductility of tungsten—a review *Int. J. Refract. Metals Hard Mater.* 75 170–83
- [12] Reiser J., Rieth M., Dafferner B. and Hoffmann A. 2012 Tungsten foil laminate for structural divertor applications—basics and outlook *J. Nucl. Mater.* 423 1–8
- [13] Chen C., Qian S., Liu R., Wang S., Liao B., Zhong Z., Cao L., Coenen J.W. and Wu Y. 2019 The microstructure and tensile properties of W/Ti multilayer composites prepared by spark plasma sintering *J. Alloys Compd.* 780 116–30
- [14] Waseem O.A. and Ryu H.J. 2016 Tungsten-Based Composites for Nuclear Fusion Applications (Rijeka: Intech)
- [15] Zhang L.H., Jiang Y., Fang Q.F., Zhang T., Wang X.P. and Liu C.S. 2016 Toughness and microstructure of tungsten fibre net-reinforced tungsten composite produced by spark plasma sintering *Mater. Sci. Eng.* A 659 29–36
- [16] Mao Y. et al 2018 Influence of the interface strength on the mechanical properties of discontinuous tungsten fiberreinforced tungsten composites produced by field assisted sintering technology Composites A 107 342–53
- [17] Kim J.-K. and Mai Y.-W. 1998 Engineered Interfaces in Fiber Reinforced Composites (Amsterdam: Elsevier)
- [18] Du J., Höschen T., Rasinski M., Wurster S., Grosinger W. and You J.-H. 2010 Feasibility study of a tungsten wire-reinforced tungsten matrix composite with ZrO<sub>x</sub> interfacial coatings *Compos. Sci. Technol.* 70 1482–9
- [19] Riesch J., Buffiere J.-Y., Höschen T., di Michiel M., Scheel M., Linsmeier C. and You J.-H. 2013 *In situ* synchrotron tomography estimation of toughening effect by semi-ductile fibre reinforcement in a tungsten-fibre-reinforced tungsten composite system *Acta Mater.* 61 7060–71
- [20] Gietl H., Riesch J., Coenen J.W., Höschen T., Linsmeier C. and Neu R. 2017 Tensile deformation behavior of tungsten fibrereinforced tungsten composite specimens in as-fabricated state Fusion Eng. Des. 124 396–400

- [21] Mao Y. et al 2017 Development and characterization of powder metallurgically produced discontinuous tungsten fiber reinforced tungsten composites Phys. Scr. T170 014005
- [22] Mao Y. *et al* 2020 Development of tungsten fiber-reinforced tungsten with a porous matrix *Phys. Scr.* **T171** 014030
- [23] Jasper B. et al 2016 Behavior of tungsten fiber-reinforced tungsten based on single fiber push-out study Nucl. Mater. Energy 9 416–21
- [24] Zok F.W. and Levi C.G. 2001 Mechanical properties of porousmatrix ceramic composites Adv. Eng. Mater. 3 15–23
- [25] Brezinsek S. 2015 Plasma-surface interaction in the Be/W environment: conclusions drawn from the JET-ILW for ITER J. Nucl. Mater. 463 11–21
- [26] De Temmerman G., Baldwin M.J., Doerner R.P., Nishijima D., Seraydarian R. and Schmid K. 2009 Insight into the codeposition of deuterium with beryllium: influence of the deposition conditions on the deuterium retention and release J. Nucl. Mater. 390–391 564–7
- [27] Kreter A., Buzi L., De Temmerman G., Dittmar T., Doerner R.P., Linsmeier C., Nishijima D., Reinhart M. and Unterberg B. 2014 Fuel retention and erosion of metallic plasma-facing materials under the influence of plasma impurities 25th IAEA Fusion Energy Conf. (St. Petersburg, Russia, 13–18 October 2014) (https://www-pub.iaea.org/iaeameetings/46091/25thfusion-energy-conference-fec-2014)
- [28] Kreter A., Brandt C., Huber A., Kraus S., Möller S., Reinhart M., Schweer B., Sergienko G. and Unterberg B. 2015 Linear plasma device PSI-2 for plasma-material interaction studies *Fusion Sci. Technol.* 68 8–14
- [29] Riesch J. et al 2016 Properties of drawn W wire used as high performance fibre in tungsten fibre-reinforced tungsten composite IOP Conf. Ser.: Mater. Sci. Eng. 139 012043
- [30] Riesch J., Han Y., Almanstötter J., Coenen J.W., Höschen T., Jasper B., Zhao P., Linsmeier C. and Neu R. 2016 Development of tungsten fibre-reinforced tungsten composites towards their use in DEMO-potassium doped tungsten wire *Phys. Scr.* T167 014006
- [31] Mao Y. et al 2019 On the nature of carbon embrittlement of tungsten fibers during powder metallurgical processes Fusion Eng. Des. 145 18–22
- [32] Wirtz M., Uytdenhouwen I., Barabash V., Escourbiac F., Hirai T., Linke J., Loewenhoff T., Panayotis S. and Pintsuk G. 2017 Material properties and their influence on the behaviour of tungsten as plasma facing material *Nucl. Fusion* 57 066018
- [33] Salançon E., Dürbeck T., Schwarz-Selinger T., Genoese F. and Jacob W. 2008 Redeposition of amorphous hydrogenated carbon films during thermal decomposition *J. Nucl. Mater.* 376 160–8

- [34] Huber A. et al 2014 Investigation of the impact of transient heat loads applied by laser irradiation on ITER-grade tungsten Phys. Scr. T159 014005
- [35] Eckstein W. 2002 Calculated Sputtering, Reflection and Range Values (Germany: Max-Planck-Institut für Plasmaphysik) p 224
- [36] Tu H., Wang S., Cui L., Cheng L., Lu G.-H., O'Connor D.J. and Shi L. 2021 The influence of impurities on the erosion of tungsten by low energy high flux deuterium plasma irradiation J. Nucl. Mater. 556 153168
- [37] Doerner R.P., Baldwin M.J. and Nishijima D. 2014 Plasmainduced morphology of beryllium targets exposed in PISCES-B J. Nucl. Mater. 455 1–4
- [38] Kreter A. et al 2008 Effect of surface roughness and substrate material on carbon erosion and deposition in the TEXTOR tokamak Plasma Phys. Control. Fusion 50 095008
- [39] Hakola A. et al 2014 Long-term erosion of plasma-facing materials with different surface roughness in ASDEX Upgrade Phys. Scr. T159 014027
- [40] Doerner R.P., Baldwin M.J., De Temmerman G., Hanna J., Nishijima D., Roth J., Schmid K., Tynan G.R. and Umstadter K. 2009 Codeposition of deuterium with ITER materials Nucl. Fusion 49 035002
- [41] De Temmerman G. and Doerner R.P. 2009 Deuterium retention and release in tungsten co-deposited layers *J. Nucl. Mater.* **389** 479–83
- [42] Tanabe T. 2014 Review of hydrogen retention in tungsten *Phys. Scr.* T159 014044
- [43] Bird R., Stewart W. and Lightfoot E. 2007 *Transport Phenomena* 2nd edn (New York: Wiley)
- [44] Ueda Y. et al 2017 Baseline high heat flux and plasma facing materials for fusion Nucl. Fusion 57 092006
- [45] Linke J. et al 2011 Performance of different tungsten grades under transient thermal loads Nucl. Fusion 51 073017
- [46] Wirtz M., Linke J., Loewenhoff T., Pintsuk G. and Uytdenhouwen I. 2016 Thermal shock tests to qualify different tungsten grades as plasma facing material *Phys.* Scr. T167 014015
- [47] Wirtz M., Cempura G., Linke J., Pintsuk G. and Uytdenhouwen I. 2013 Thermal shock response of deformed and recrystallised tungsten *Fusion Eng. Des.* 88 1768–72
- [48] Lake G.J. and Yeoh O.H. 1987 Effect of crack tip sharpness on the strength of vulcanized rubbers J. Polym. Sci. B 25 1157–90
- [49] Terentyev D., Gaganidze E., Klimenkov M., Coenen J.W., Zinovev A., Rieth M. and Pintsuk G. 2021 Properties of neutron irradiated tungsten: recent lessons 18th Int. Conf. Plasma-Facing Materials and Components for Fusion Applications (17–21 May 2021) (https://www.fz-juelich.de/ conferences/pfmc-18)